

INFLUENCE OF ANGULAR MOMENTUM AND COULOMB INTERACTION OF COLLIDING NUCLEI ON THEIR MULTIFRAGMENTATION

A. Ergun, H. Imal, N. Buyukcizmeci, and R. Ogul
Department of Physics, University of Selçuk, 42079 Konya, Turkey

A.S. Botvina

*Institute for Nuclear Research, Russian Academy of Sciences, 117312 Moscow, Russia and
Frankfurt Institute for Advanced Studies, J.W. Goethe University, D-60438 Frankfurt am Main, Germany*

(Dated: March 2, 2022)

Theoretical calculations are performed to investigate the angular momentum and Coulomb effects on fragmentation and multifragmentation in peripheral heavy-ion collisions at Fermi energies. Inhomogeneous distributions of hot fragments in the freeze-out volume are taken into account by microcanonical Markov chain calculations within the Statistical Multifragmentation Model (SMM). Including an angular momentum and a long-range Coulomb interaction between projectile and target residues leads to new features in the statistical fragmentation picture. In this case, one can obtain specific correlations of sizes of emitted fragments with their velocities and an emission in the reaction plane. In addition, one may see a significant influence of these effects on the isotope production both in the midrapidity and in the kinematic regions of the projectile/target. The relation of this approach to the simulations of such collisions with dynamical models is also discussed.

PACS numbers: 25.70.-z, 25.70.Pq

I. INTRODUCTION

It has been commonly accepted since long ago that in central heavy-ion collisions at Fermi energies (20–50 MeV per nucleon) relatively high excitation energies of nuclear matter, with temperatures up to $T \approx 5\text{--}8$ MeV, can be reached [1]. Therefore, they become a suitable tool to study the equation of state (EoS) of hot nuclear matter and the nuclear liquid-gas phase transitions at subnuclear densities. As discussed previously [2], with the help of multifragmentation one can study the properties of hot fragments in the vicinity of other nuclear species. The angular momentum effect is usually disregarded in this case, since the impact parameters are small. During the peripheral heavy-ion collisions at the same energies, a considerable amount of angular momentum could be transferred from the interaction region to the excited projectile and target residual nuclei, and this can lead to significant changes in their multifragmentation [3–5]. Additional long-range forces caused by the complicated Coulomb interaction between the target and projectile-like sources are involved essentially in the process [5, 6]: The multifragmentation in the presence of the external Coulomb field offers a possibility to study, experimentally, the effects of this long-range force, which are very important for disintegration of matter [4]. This is also necessary for construction of a reliable EoS of nuclear matter at subnuclear densities. Another motivation of these studies is that similar conditions for nuclear matter take place during the collapse and explosion of massive stars and in the crust of neutron stars [7, 8], where the Coulomb interactions of dense electron environment change the fragmentation picture. It is generally assumed that the statistical equilibrium regarding the fragment composition at subnuclear densities should

be established in these astrophysical cases. Therefore, the analysis of the observables obtained in laboratory experiments with statistical models is a proper way to get knowledge on stellar matter. Previous studies of isospin composition of the produced fragments were found to be especially important for determining the strength of the symmetry energy during fragment formation in hot and diluted environments [2, 9–11].

In the analysis of ALADIN data, charge and isotope yields, fragment multiplicities and temperatures, and correlations of various fragment properties were successfully described by statistical ensemble approach [11–16] within the Statistical Multifragmentation Model (SMM) [17]. This was also achieved in the analysis of the experimental data of Liu et al. [18] obtained at the MSU laboratory at 50 MeV/nucleon [19–21], and in the analysis of TAMU data [22, 23]. In these studies, the symmetry energy of fragments was one of the main model parameters governing the mean N/Z values, the isoscaling parameters, and the isotopic composition of the fragments. For interpretation of ALADIN and MSU experiments, which can be explained by formation and decay of single thermalized sources, we considered the averaged Coulomb interaction of fragments (the Wigner-Seitz approximation), since a direct positioning of fragments in the freeze-out volume has minor influence on their charge and isotope distributions. This is well justified for relativistic peripheral collisions, and central collisions of heavy nuclei around the Fermi energy. However, important information on multifragmentation and properties of fragments can be extracted in peripheral collisions at Fermi energies as well. The new fragment partitions can be obtained by including the Coulomb effects caused by the proximity of colliding target and projectile nuclei, as well as the effects by large angular momentum

transfer to the multifragmenting sources. For example, a long-range Coulomb interaction of the target- and projectile-like sources changes the fragmentation pattern and leads to a predominant midrapidity (neck-like) emission of light and intermediate mass fragments (IMF, with charge numbers $Z = 3-20$). Few such experiments have already been analyzed with statistical models [23, 24]. However, there were no systematic theoretical investigations of the Coulomb and angular momentum effects on multifragmentation picture at these reactions, especially on the isotope yields which are crucial for astrophysical applications. As it was suggested in Ref. [5, 6], the angular momentum may lead to more neutron-rich IMF production and to anisotropic emission with respect to the projectile and target sources.

In this paper, we shall theoretically investigate the influence of angular momentum and Coulomb interactions on the charge yields, the neutron to proton ratios and the velocity distributions of hot particles for peripheral $^{84}\text{Kr}+^{84}\text{Kr}$ collisions at 35 MeV per nucleon. We believe that this is a quite typical reaction, and our selection is partly motivated by recent FAZIA experiments [25]. For the simulation of the reactions, we consider the break-up of a single source ^{84}Kr in the proximity of a secondary source ^{84}Kr , as a symmetric system in terms of isospin contents. The calculations are carried out within the Markov chain version of the statistical multifragmentation model, which is designed for a microcanonical simulation of the decay modes of nuclear sources [5, 26]. This method is based on producing the Markov chain of partitions which characterize the whole statistical ensemble. In this method the individual fragment partitions and coordinate positions of fragments in the freeze-out volume are generated. They are selected by the Metropolis algorithm and we can take into account the influences of angular momentum and Coulomb interactions for each spatial configuration of primary fragments in the freeze-out volume, similar to Refs. [3, 4].

II. STATISTICAL APPROACH TO MULTIFRAGMENTATION

It is assumed in the microcanonical SMM that a statistical equilibrium is reached at low density freeze-out region. The breakup channels are composed of nucleons and nuclear fragments, and the laws of conservation of energy E_x , momentum, angular momentum, mass number A and charge number Z are considered. Besides the breakup channels, the compound-nucleus channels are also included, and competition between all channels is permitted. In this way, the SMM covers the conventional evaporation and fission processes occurring at low excitation energy as well as the transition region between the low and high energy de-excitation regimes. In the thermodynamic limit, SMM is consistent with liquid-gas phase transitions when the liquid phase is represented by infinite nuclear clusters [27], that allow connections

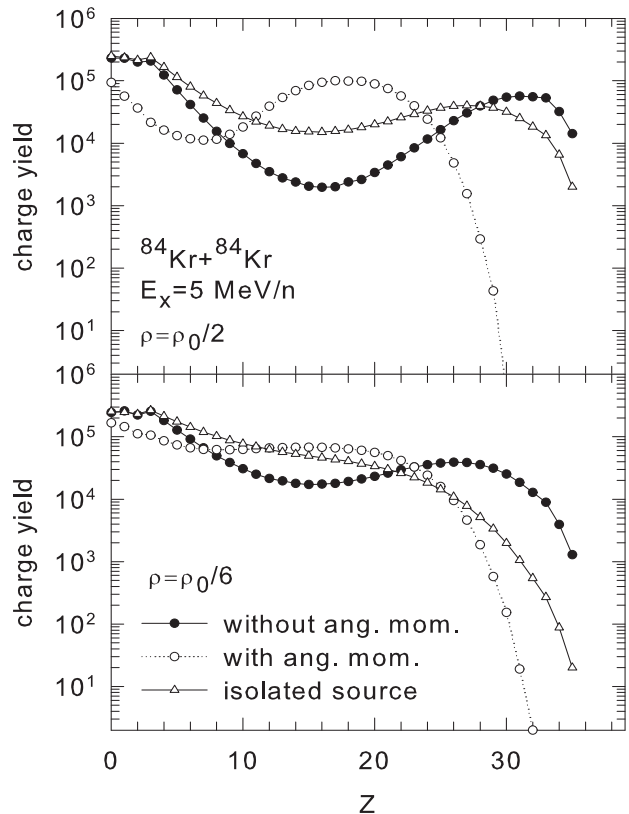


FIG. 1: Total charge yield of primary hot fragments, in the cases of without (full circles) and with angular momentum (open circles, $L = 80\hbar$), after multifragmentation of the projectile ^{84}Kr source at the excitation energy $E_x = 5$ MeV/nucleon. This source is assumed to be formed in the peripheral $^{84}\text{Kr} + ^{84}\text{Kr}$ collision at 35 MeV/nucleon, and its disintegration is affected by the Coulomb field of the target source. Top and bottom panels show the results at freeze-out densities $\rho = \rho_0/2$, and $\rho = \rho_0/6$, respectively. For comparison, the results of multifragmentation of a single isolated ^{84}Kr source, at the same excitation energy but without the external Coulomb field and without angular momentum, are shown too.

for the astrophysical cases [28]. We calculate the statistical weights of all breakup channels partitioning the system into various species. The decay channels are generated by Monte Carlo method according to their statistical weights. In the Markov chain SMM [5, 26] we use also ingredients taken from the standard SMM version developed in the Refs. [17, 29, 30] which was successfully used for comparison with various experimental data: Light fragments with mass number $A \leq 4$ and charge number $Z \leq 2$ are considered as elementary particles with the corresponding spins (nuclear gas) that have translational degrees of freedom. The fragments with mass number $A > 4$ are treated as heated nuclear liquid drops. In this way one can study the nuclear liquid-gas coexistence in the freeze-out volume. Free energies $F_{A,Z}$ of each frag-

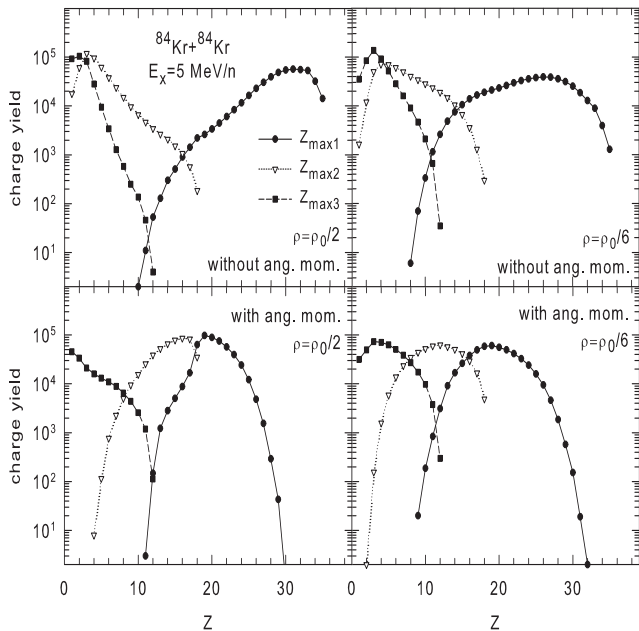


FIG. 2: Charge yield of the first, second and third largest hot fragments (Z_{max1} , Z_{max2} , and Z_{max3}) after multifragmentation of the ^{84}Kr source (as in Fig. 1). Top panels show the results without angular momentum, and bottom panels with angular momentum ($L = 80\hbar$).

ment are parameterized as a sum of the bulk, surface, Coulomb and symmetry energy contributions

$$F_{A,Z} = F_{A,Z}^B + F_{A,Z}^S + E_{A,Z}^C + E_{A,Z}^{sym}. \quad (1)$$

The bulk contribution is given by $F_{A,Z}^B = (-W_0 - T^2/\varepsilon_0)A$, where T is the temperature, the parameter ε_0 is related to the level density, and $W_0 = 16$ MeV is the binding energy of infinite nuclear matter. Contribution of the surface energy is $F_{A,Z}^S = B_0 A^{2/3} [(T_c^2 - T^2)/(T_c^2 + T^2)]^{5/4}$, where $B_0 = 18$ MeV is the surface energy term, and $T_c = 18$ MeV the critical temperature of the infinite nuclear matter. In the standard SMM version the Coulomb energy contribution is $E_{A,Z}^C = cZ^2/A^{1/3}$, where c denotes the Coulomb parameter obtained in the Wigner-Seitz approximation, $c = (3/5)(e^2/r_0)(1 - (\rho/\rho_0)^{1/3})$, with the charge unit e , $r_0 = 1.17$ fm, and ρ_0 is the normal nuclear matter density (0.15 fm^{-3}). However, within this Markov-chain SMM we directly calculate the Coulomb interaction of non-overlapping fragments in the freeze-out by taking into account their real coordinate positions. The symmetry term is $E_{A,Z}^{sym} = \gamma(A - 2Z)^2/A$, where $\gamma = 25$ MeV is the symmetry energy parameter. All the parameters given above are taken from the Bethe-Weizsaecker formula and correspond to the assumption of isolated fragments with normal density unless their modifications in the hot and dense freeze-out configuration follow the analysis of experimental data. For the freeze-out density, one-third of normal nuclear matter

density is assumed in many successful studies and consistent with independent experimental determination in sources formed in peripheral nuclear collisions [31, 32]. To be more general, in this work we use $\rho = \rho_0/2$ and $\rho = \rho_0/6$ densities for better evaluation of Coulomb and angular momentum effects. The different positioning of particles and volume parameters is also useful for understanding the origin of the kinetic energies of fragments observed in experimental data. In the case of the large density ($\rho = \rho_0/2$) we assume a deformation of fragments in the freeze-out volume by effectively reducing distances between the fragments for calculation of their Coulomb interaction by a factor of 0.7. This can be partly justified by non-spherical shape of these fragments since they are excited. Usually, we generate about 5.10^5 Monte Carlo events to provide sufficient statistics.

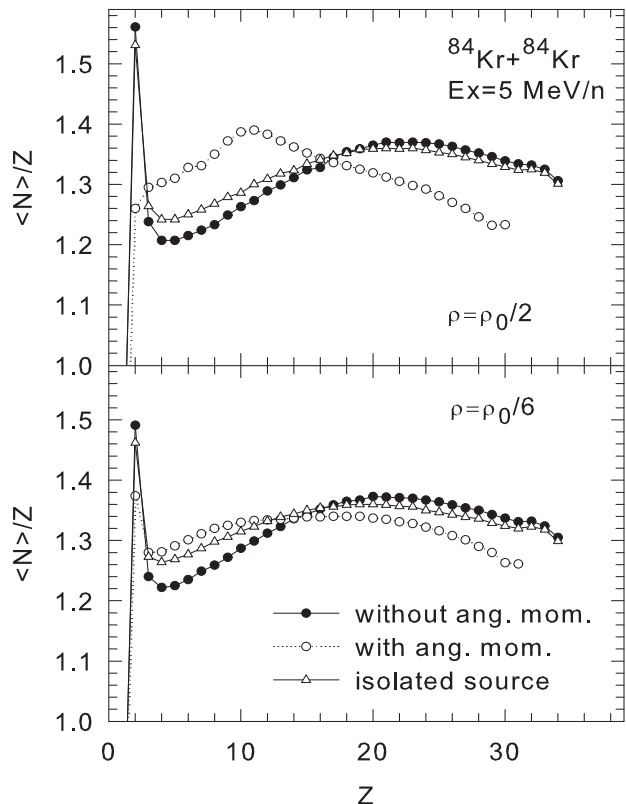


FIG. 3: The neutron-to-proton ratio $\langle N \rangle / Z$ of hot primary fragments produced at the freeze-out density $\rho = \rho_0/2$ (top panel) and $\rho = \rho_0/6$ (bottom panel). Other notations are as in Fig. 1.

III. EFFECTS OF ANGULAR MOMENTUM AND COULOMB INTERACTION OF PROJECTILE AND TARGET LIKE SOURCES

As was mentioned, we analyze peripheral nucleus-nucleus collisions at 35 MeV/nucleon with the corre-

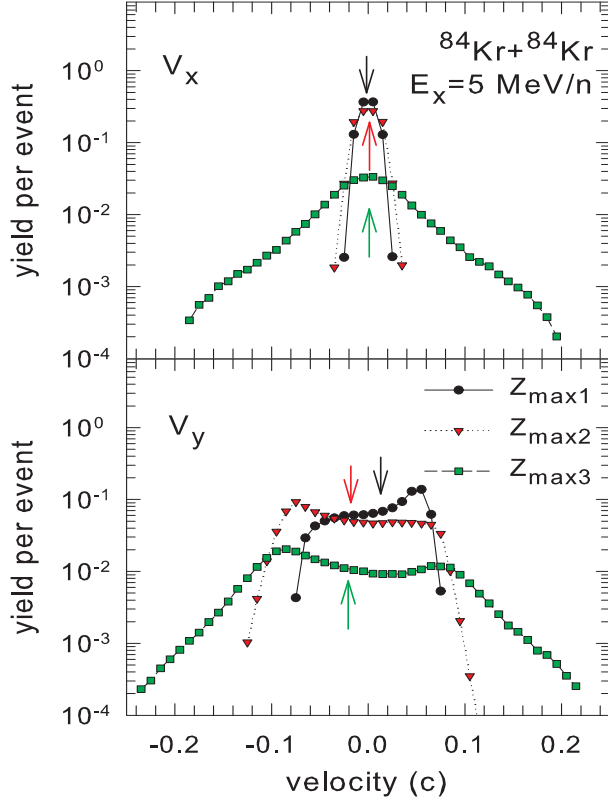


FIG. 4: (Color online) V_x and V_y velocity distributions of the first, second and third largest fragments in multifragmentation of ^{84}Kr with the angular momentum $L = 80\hbar$ and at the freeze-out density $\rho = \rho_0/2$.

sponding relative velocity between the projectile and target about 80 mm/ns. At the initial dynamical stage of such a collision, the projectile nucleons interact with target nucleons and some energetic products of this interaction can leave the nuclei as pre-equilibrium particles. The kinetic energy of colliding nuclei can also be converted into the excitation energy of projectile and target residues. Therefore, the relative velocity between the residues decreases as well. These excited target and projectile-like sources decay afterwards.

It is known that nuclear multifragmentation is a fast process within a characteristic time around 100 fm/c. Therefore, projectile and target-like sources will not be far from each other before disintegration. The idea is that at these short distances the long range Coulomb field of one of the sources influences the break up of the other one. In this case we are dealing with the multifragmentation in a double nuclear system, that is a new physical situation with respect to the standard multifragmentation of a single isolated source.

According to our estimates from the energy conservation, their relative velocity should decrease to ~ 50 mm/ns, at an excitation energy around 5 MeV/nucleon

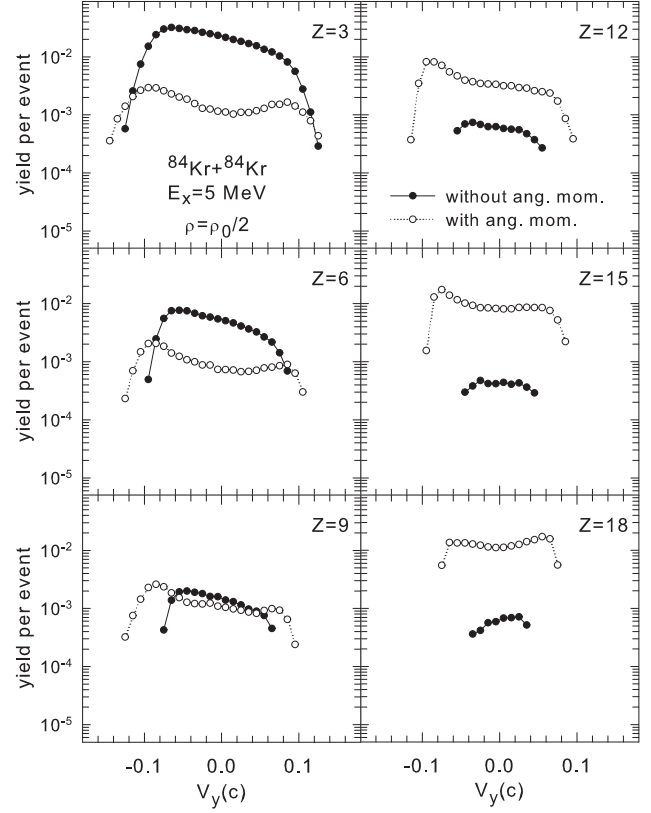


FIG. 5: The relative yields of specific fragments (see panels) coming from the disintegration of ^{84}Kr projectile source at the excitation energy of 5 MeV/nucleon as a function of the velocity V_y in the source frame. The calculations have been performed with (open circles for $L = 80\hbar$), and without angular momentum (full circles) at the freeze-out density $\rho = \rho_0/2$.

transferred to the residues. In this case, they will be separated by ≈ 15 fm in a time of 100 fm/c. The decay of the two excited sources in such a double system is determined by the short-range nuclear forces. However, the presence of an external Coulomb field (for each source) can affect the composition of the produced fragments and their relative positions. In particular, an additional Coulomb barrier will prevent disintegration of the sources into many small pieces. It should be noted that during the evolution of a double system we must take into account its total center of mass conservation without a separate constraint in the freeze-out volumes of disintegrating sources. On the other hand, we include the angular momenta (rotation) of the separate sources, which can be transferred after the collision. It will also influence the positions and sizes of the fragments at the freeze-out [3, 5, 6].

In the following we demonstrate the results for multifragmentation of the projectile-like source (we call it the first source) by assuming the Coulomb field coming from the center of the target source (the second source).

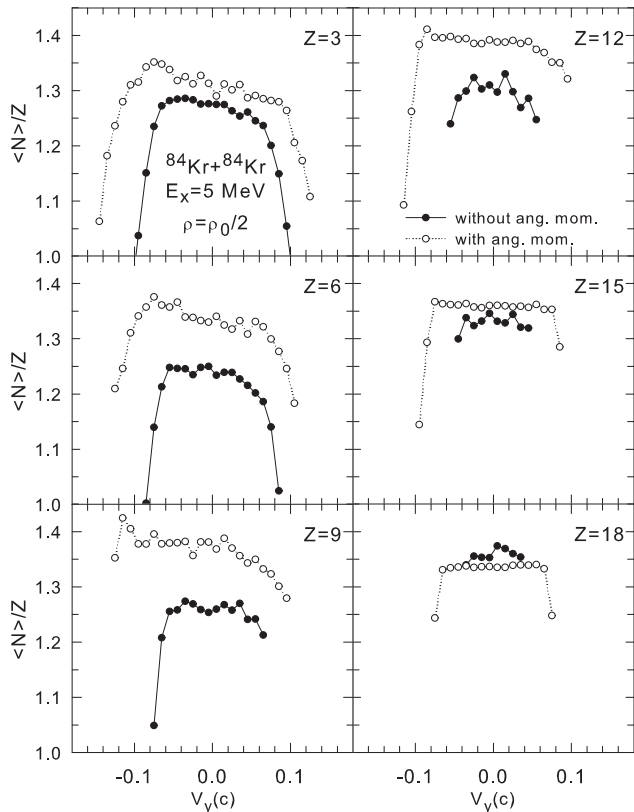


FIG. 6: Average neutron to proton ratios as a function of V_y shown in Fig. 5 (notations are the same).

The first source is assumed to fly along Y -axis, and the second one is in the opposite direction (related to the center of mass of the double system). This separation axis may slightly deviate from the initial beam axis. The location of the second source is taken as $R_Y = -10.6$ fm and $R_Z = 10.6$ fm with respect to the first source. The peripheral collision is assumed to take place in the $Y-Z$ plane, therefore, the coordinates in Z -axis is determined by the sizes of colliding nuclei, as well as by their possible repulsion after the collision. The X -axis is assumed to be an angular momentum axis. We suggest that this relative space configuration of the sources is quite general and suitable for investigating the Coulomb and angular momentum effects.

The pre-equilibrium emission of few nucleons during the dynamical stage may decrease the excitation energy and relative velocity of the residues. However, this can be accounted in the statistical approach by changing the corresponding input and by using the ensemble of the sources (see, e.g., [11]) with adequate parameters. On the other hand, as was shown by many theoretical and experimental works (see, e.g., [12, 17, 33]), the relative yields of IMF do not depend much on the size of the sources in the multifragmentation regime (a scaling effect). Therefore, for our purposes it is sufficient to con-

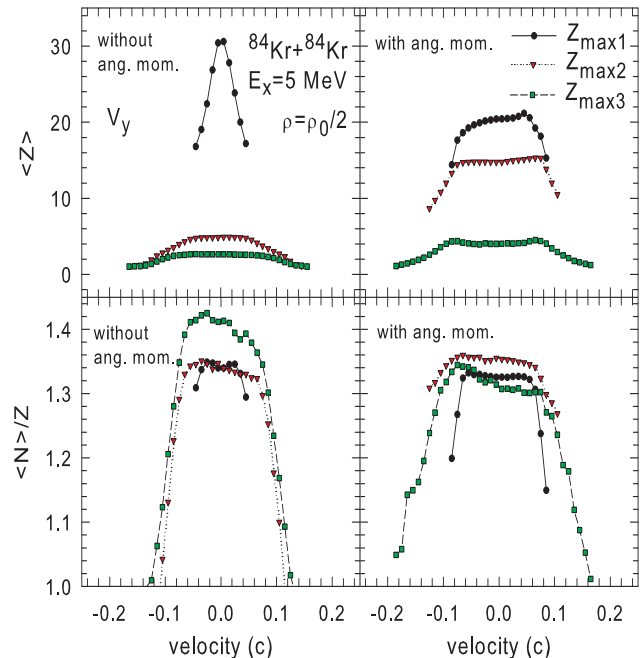


FIG. 7: (Color online) Average charge Z (top panels) and $\langle N \rangle / Z$ (bottom panels) distributions of the first, second and third largest hot fragments (Z_{max1} , Z_{max2} , and Z_{max3}) after multifragmentation of ^{84}Kr projectile source at $E_x = 5$ MeV/nucleon versus V_y in the source frame. The freeze-out density is $\rho = \rho_0/2$. Left panels represent the results without angular momentum, while the right panels with angular momentum ($L = 80\hbar$).

sider the sources of the same size and isospin content as the colliding nuclei (^{84}Kr).

A. Charge Distributions

The purpose of our analysis is to understand the new characteristics of fragment distributions, which are important for interpretation of many experiments on heavy-ion collisions at Fermi energies. We shall study the angular momentum and Coulomb field influences on the charge and isospin contents of produced fragments, and compare them with the standard calculations without these effects. It is expected that the correlations of the sizes and $\langle N \rangle / Z$ of hot fragments with their velocities will be important. For this purpose, after the breakup of the sources we calculate the Coulomb propagation of produced hot fragments by taking into account the Coulomb interactions of particles in the double system and their velocities at the break-up time. In this paper, in order to clarify the modification of the multifragmentation picture caused by the new effects, we do not apply the secondary de-excitation of the hot fragments which, however, can lead to important consequences especially for isospin composition of final fragments.

In Fig. 1, we show the total charge yields of hot fragments in case of with and without angular momentum conservation. Angular momentum value of $80\hbar$ is selected as an upper estimate. It is seen that the charge distributions are very sensitive to the freeze-out densities. An angular momentum favors emission of large nearly symmetric fragments (like a nuclear fission) since the system in the freeze-out needs to have a large moment of inertia in order to minimize the rotational energy and to maximize the entropy. It is in a competition with the second source through the Coulomb interaction which prevents to emit an IMF with a large charge number. The latter can be seen clearly in comparison with the case of the fragmentation of a standard single isolated source.

For more details, we show in Fig. 2 the yield distributions of the first, second and third largest fragments versus their charge numbers Z_{max1} , Z_{max2} , and Z_{max3} , respectively. These observables are used to obtain a complementary information about the fragmentation pattern. Top panels include the long-range Coulomb contribution from the second source only, and bottom panels include, in addition, the angular momentum effects. It is obvious that the distributions of Z_{max1} , Z_{max2} , and Z_{max3} are ordered according to their size. In the case of including angular momentum (bottom panels), average value of Z_{max1} decreases, while Z_{max2} and Z_{max3} show an increasing trend. A small freeze-out density ($\rho = \rho_0/6$) leads to the smoother and broader distributions (sometimes Gaussian-like ones) caused by the less restricted population of the larger coordinate phase space.

B. $\langle N \rangle / Z$ and Velocity Distributions

The initial value of neutron-to-proton ratio (N/Z) of the source ^{84}Kr is 1.33. In Fig. 3, we show that angular momentum leads to increasing N/Z values of IMFs in the case of strongly asymmetric decay. It is also caused by the increasing moment of inertia of the system that favors a bigger phase space of the reaction [5]. It is a very instructive trend which can be responsible for many isospin observables.

In Fig. 4, we present the yields per event as a function of the velocities V_x and V_y for the fragments having first, second and third biggest charge numbers. The V_x velocity distributions in the direction of the angular momentum are shown in the top panel. The first and second fragments are nearly peaked around 0, and it means that they are emitted mostly in $V_y - V_z$ plane. This is very different from the case of isotropic statistical emission taking place without angular momentum, and which is sometimes simply assumed as the only possibility for the statistical break-up. In our case all these fragments fly predominantly in the plane of rotation, even though the smallest fragments can deviate from this plane. Another important effect can be seen in the bottom panel of Fig. 4. We remind that the velocity V_y determines

the separation axis (close to the beam axis), where the sources move in opposite directions. One can see that there is an order in the emission of fragments of different sizes, such that the largest fragments have the largest velocity V_y , which is bigger than those of the second and third ones. The arrows refer to the average values of the velocity distributions. The maximum fragments fly predominantly in the forward direction as $V_y > 0$, while the second and third ones fly to backward direction as $V_y < 0$ (i.e., to the direction of the target source), and in this way they may simulate the so-called 'midrapidity emission'. This is the consequence of the fragment coordinate positions occupied predominantly in the freeze-out, and this is caused mainly by the Coulomb repulsion of the second source. This effect is consistent with the previous experimental observations [34]. Its dynamical interpretation may also be possible, however, the contribution of the Coulomb interaction was not separated and not investigated up to now with dynamical models.

For detailed examination of the characteristics of produced particles, we show in Fig. 5, the relative yields (normalized per total number of generated events) of the hot primary fragments with $Z=3, 6, 9, 12, 15$, and 18 versus their velocities along the separation axis V_y . As in Fig. 4, these velocities are calculated with respect to the projectile source, so that $V_y < 0$ means an emission towards the midrapidity. The figure demonstrates clearly the predominant 'backward' emission for the light IMF with changing to 'uniform-like' emission for larger fragments. It is very important to investigate the isospin content of these fragments. Their $\langle N \rangle / Z$ ratio versus V_y is demonstrated in Fig. 6. One can see in this figure that including angular momentum can lead to increasing $\langle N \rangle / Z$ ratio for small fragments. The external Coulomb field leads to the emission of neutron-rich fragments towards the midrapidity. This trend is clearly seen for $Z=3, Z=6$, and $Z=9$. The secondary decay of such fragments may preserve the enhanced neutron content and lead to emission of final neutron-rich nuclei in the 'neck' direction. However, this explanation may not be obvious for very small species ($Z \lesssim 3$) because of their low contribution in partitions with large angular momentum, and because their preequilibrium emission is also possible in the reactions. Large species ($Z \gtrsim 15$) lose this sensitivity and they are emitted more uniformly. Including angular momentum increases also velocities of all fragments, and the distributions become broader. The drop of $\langle N \rangle / Z$ at high velocities, actually, for fragments with low yields, is trivially explained by strong Coulomb acceleration if the mass is small.

For completeness, we present how the average charge $\langle Z \rangle$ (top panels) and $\langle N \rangle / Z$ of the fragments with Z_{max1} , Z_{max2} , and Z_{max3} change with V_y in Fig. 7, for the cases of with and without angular momentum effect. It is in agreement with our previous conclusions on modification of statistical picture. In particular, one can see a trend of increasing $\langle N \rangle / Z$ towards the midrapidity for Z_{max2} and Z_{max3} (bottom panels).

To verify our new-found trends we also performed the same calculations for heavier systems, e.g., $^{197}\text{Au}+^{197}\text{Au}$ collisions. In all cases, we have got the same qualitative modifications of the standard multifragmentation picture.

IV. RELATION BETWEEN STATISTICAL AND DYNAMICAL DESCRIPTIONS

In this paper we investigate the kinematic characteristics, sizes and isospin properties of hot fragments. Subsequently, these fragments will be de-excited by emission of light particles, or by the secondary break-up, during their propagation. As was shown in many previous works the secondary process can be reliably described within statistical models (see, e.g., Refs. [11, 17] and references in). One of the outstanding problems under discussion is if dynamical models alone can describe the same evolutionary scenario leading to equilibration and multifragmentation as assumed by statistical models. In other words, is it possible to use only a dynamical description, instead of subdividing the whole reaction into dynamical and statistical stages? Some dynamical approaches try to reach this goal starting from 'first principles' like Fermionic molecular dynamics (FMD) [35], and antisymmetrized molecular dynamics (AMD) [36]. Other approaches, like QMD [37] and BNV [38, 39] use semi-classical equations including two-body collisions and some elements of stochasticity. In all cases dynamical simulations are more complicated and time-consuming as compared with statistical models. This is why full calculations, e.g. with FMD and AMD models, can only be done for relatively light systems. This prevents using these codes in many cases of nuclear fragmentation. A natural solution of this problem is to develop hybrid approaches which combine dynamical models for describing the nonequilibrium early stages of the reaction with statistical models for describing the fragmentation of equilibrated sources. In this respect, the statistical and dynamical approaches are complementary and suitable for many practical calculations, which are required, e.g., in medicine, space research, and other fields.

One can try dynamical model to describe the fragment (i.e., nucleon cluster) formation at the time of the nuclear freeze-out (~ 100 fm/c) too, as we are doing for hot fragments with statistical models. Actually, it is popular to explain in a dynamical way the formation of neck-like fragments in collisions of heavy ions around the Fermi energy [38]. However, the essential problem in the dynamical approach is the connection to the relatively slow secondary de-excitation stage of the fragment ($\gtrsim 10^2 - 10^3$ fm/c). This last stage is very important for isotope composition of final cold fragments, which may give access to the symmetry energy of nuclei and nuclear matter. As shown in some dynamical calculations [38], the primary nucleon clusters may have a low density and unusual form. So it is difficult to establish an excitation

energy of such clusters [18]. Moreover, a bigger problem is the evaluation of other properties of these clusters, such as their masses, level densities, and symmetry energies. The last ones are crucially important for the subsequent de-excitations leading to cold nuclei. To our knowledge, nobody has ever described realistically these properties within transport dynamical models. Therefore, the de-excitation results for isotope composition of final nuclei become not very reliable, and, usually, the predictions of dynamical models are limited by hot fragments. On the other hand, one can easily resolve this problem within the statistical approach. As demonstrated in Refs. [10–12] one can connect the freeze-out properties of hot fragments with their secondary de-excitation and the yield of final isotopes. In this respect, the application of appropriate statistical models to the reactions, which were considered previously only as dynamical processes, opens real chances for involving new data in theoretical analysis. One should bear in mind that the statistical and dynamical approaches are derived from different physical principles. The time-dependent dynamical approaches are based on Hamiltonian dynamics (the principle of minimal action), whereas the statistical models employ the principle of uniform population of the phase space. Actually, these two principles represent complementary methods for describing the physical reality. Therefore, a decision of using statistical or dynamical approaches for the description of nuclear multifragmentation should be made after careful examination of the degrees of equilibration expected in particular cases, and it can only be justified by the comparison with experiment.

In the case of equilibrated sources, the predictions of statistical models are usually in better agreement with experimental data. This is well known in multifragmentation of relativistic projectiles [15, 16, 40], especially when the chemical equilibrium is established in such reactions, and this equilibrium can be seen in isotopic yields [10, 11]. This can also be seen by describing the isospin observables in nucleus-nucleus collisions at lower (Fermi) energies: For example, one can compare dynamical [18] and statistical [19, 21, 41] analyses of the MSU experimental data. As shown in the present work, the effect of increasing the neutron number in IMF emitted towards the midrapidity region may also be explained within the statistical picture modified by including the external Coulomb field and angular momentum. In order to distinguish dynamical and statistical mechanisms one should involve specific isotopic experimental characteristics. For example, there are experimental data demonstrating the trend of increasing neutron richness of IMF in collisions of nuclei with increasing centrality, i.e. with increasing excitation energy, both in the 'neck region' [42] and in the single equilibrated central source [33]. Both trends can easily be explained within the statistical framework [5, 12, 33] because of the enhanced disintegration of nuclei at high excitations into more neutron-rich IMF, while a dynamical calculation predicts more neutron-rich IMF in very peripheral colli-

sions since the neutron-rich periphery of nuclei influences the dynamics of IMF formation [38]. We believe that the presented generalization of the statistical approach is very useful for the analysis of coming novel experiments aimed predominantly at measuring isotopes at low and intermediate energy collisions [25, 43]. As it was extensively discussed in Ref. [4], some 'dynamical' behaviour of many-body systems constraint by the conservation laws and influenced by the long-range forces may be simulated within the microcanonical statistical ensemble.

V. CONCLUSIONS

In conclusion, within the statistical approach we have investigated isotopic characteristics of hot fragments after the multifragmentation of the Kr-like projectiles in peripheral $^{84}\text{Kr}+^{84}\text{Kr}$ collisions around the Fermi energy. It is important and new that we have taken into account Coulomb and angular momentum effects originated after the collision dynamics. We used the microcanonical Markov chain approach within the statistical multifragmentation model. It is shown that conservation of angular momentum and complicated Coulomb interactions caused by the proximity of target and projectile-like sources in the freeze-out stage produce significant changes in the multifragmentation picture. There appear new fragment formation trends, such as an asymmetry of IMF emission (predominantly towards the midrapidity), increasing the neutron content of these IMF, a correlation (ordering) of sizes and velocity of fragments, and in-plane emission of large fragments. This is instructive since in previous years it was assumed that such effects could be explained within dynamical

models only. These features may also be preserved after the secondary excitation of hot fragments for the cold fragments, similar to the previously analyzed reactions leading to the production and decay of the single isolated sources. For the future, we plan to apply this new approach to analyze the experimental data at intermediate peripheral collisions such as the FAZIA data measured in $^{84}\text{Kr}+^{124,124}\text{Sn}$ reactions at 35 Mev/nucleon [25]. Particular isotopic effects, such as the odd-even staggering of the yield of final fragments studied by FAZIA collaboration [43], can also be analysed within similar statistical approaches. Some preliminary encouraging results obtained with the help of the ensemble of residual sources were already reported [44]. This kind of investigations will show a new connection between dynamical and statistical phenomena in nuclear reactions. As expected, it may also provide us with inputs to understand the nuclear equation of state and nuclear composition, which are important to determine the properties of nuclear and stellar matter at extreme conditions and their connections to the thermodynamics of stellar matter in astrophysical events [28]. We believe that our theoretical results may be enlightening for further analysis of the experiments.

Acknowledgments

This work was supported by TUBITAK (Turkey) with project number 113F058. We thank G. Casini for stimulating discussions and help in the preparation of the manuscript. A.S.B. acknowledges also a support by HIC for FAIR (LOEWE program).

-
- [1] M. D'Agostino et al., *Phys. Lett B* **371**, 175 (1996).
 - [2] A. S. Botvina, O. V. Lozhkin, and W. Trautmann, *Phys. Rev. C* **65**, 044610 (2002).
 - [3] A. S. Botvina and D. H. E. Gross, *Nucl. Phys. A* **592**, 257 (1995).
 - [4] D. H. E. Gross, *Phys. Rep.* **279**, 119 (1997).
 - [5] A. S. Botvina, I. N. Mishustin, *Phys. Rev. C* **63**, 061601(R) (2001).
 - [6] A. S. Botvina, M. Bruno, M. D'Agostino, and D. H. E. Gross, *Phys. Rev. C* **59** 3444 (1999).
 - [7] J. M. Lattimer and M. Prakash, *Astrophys. J.* **550**, 426 (2001), and references therein.
 - [8] A. S. Botvina, I. N. Mishustin, *Nucl. Phys. A* **843**, 98 (2010).
 - [9] A. Ono, P. Danielewicz, W. A. Friedman, W. G. Lynch, and M. B. Tsang, *Phys. Rev. C* **68**, 051601(R) (2003).
 - [10] A. Le Fèvre et al., *Phys. Rev. Lett* **94**, 162701 (2005).
 - [11] R. Ogul, A. S. Botvina, U. Atav, N. Buyukcizmeci, I. N. Mishustin et al., *Phys. Rev. C* **83**, 024608 (2011).
 - [12] N. Buyukcizmeci, R. Ogul, A. S. Botvina, *Eur. Phys. J. A* **25** 57 (2005).
 - [13] A. S. Botvina et al., *Phys. Rev. C* **74**, 044609 (2006).
 - [14] A. S. Botvina and I. N. Mishustin, *Phys. Lett. B* **294**, 23 (1992).
 - [15] A. S. Botvina et al., *Nucl. Phys. A* **584**, 737 (1995).
 - [16] H. Xi et al., *Z. Phys. A* **359**, 397 (1997).
 - [17] J. P. Bondorf et al., *Phys. Rep.* **257**, 133 (1995).
 - [18] T. X. Liu et al., *Phys. Rev. C* **69**, 014603 (2004).
 - [19] R. Ogul et al., *J. Phys. G: Nucl. Part. Phys.* **36**, 115106 (2009).
 - [20] N. Buyukcizmeci et al., *Acta Physica Polonica B* **42**, 697 (2011).
 - [21] N. Buyukcizmeci et al., *J. Phys. G: Nucl. Part. Phys.* **39**, 115102 (2012).
 - [22] J. Iglío, et al., *Phys. Rev. C* **74**, 024605 (2006).
 - [23] G. A. Souliotis et al., *Phys. Rev. C* **75**, 011601(R) (2007).
 - [24] M. Jandel, A. S. Botvina et al., *Journal of Physics G: Nucl. Part. Phys.* **31**, 29 (2005).
 - [25] S. Barlini et al., *Phys. Rev. C* **87**, 054607 (2013).
 - [26] A. S. Botvina, *arXiv:nucl-th/0008068*, (2000).
 - [27] S. Das Gupta and A. Z. Mekjian, *Phys. Rev. C* **57**, 1361 (1998).
 - [28] N. Buyukcizmeci et al., *Nucl. Phys. A* **907**, 13 (2013).
 - [29] A. S. Botvina, A. S. Iljinov, I. N. Mishustin, *Sov. J. Nucl.*

- Phys.* **42**, 712 (1985).
- [30] A. S. Botvina et al., *Nucl. Phys. A* **475**, 663 (1987).
- [31] S. Fritz, et al., *Phys. Lett.* **B461**, 315 (1999).
- [32] V. E. Viola, K. Kwiatkowski, J. B. Natowitz, and S. J. Yennello, *Phys. Rev. Lett.* **93**, 132701 (2004).
- [33] P. Milazzo et al., *Phys. Rev. C* **62**, 041602 (2000).
- [34] J. Colin et al., *Phys. Rev. C* **67**, 064603 (2003).
- [35] H. Feldmeier, *Nucl. Phys. A* **681**, 398c (2001).
- [36] A. Ono, H. Horiuchi, *Phys. Rev. C* **53**, 2958 (1996).
- [37] W. Bauer, et al., *Annu. Rev. Nucl. Part. Sci.* **42**, 77 (1992); B. A. Li, *Phys. Rev. C* **47**, 693 (1993); J. Konopka, et al., *Progr. Part. Nucl. Phys* **30**, 301 (1993); M. Colonna, et al., *Nucl. Phys. A* **589**, 160 (1995); C. Fuchs, H. Wolter, *Nucl. Phys. A* **589**, 732 (1995); A. S. Botvina, et al., *Phys. At. Nucl.* **58**, 1703 (1995).
- [38] V. Baran et al., *Nucl. Phys. A* **703**, 603 (2002).
- [39] P. Napolitani, M. Colonna, F. Gulminelli, E. Galichet, S. Piantelli, G. Verde, and E. Vient, *Phys. Rev. C* **81**, 044619 (2010).
- [40] R. P. Scharenberg et al., *Phys. Rev. C* **64**, 054602 (2001).
- [41] C. B. Das et al., *Phys. Rep.* **406**, 1 (2005).
- [42] H. Xu et al., *Phys. Rev. C* **65**, 061602 (2002).
- [43] S. Piantelli et al., *Phys. Rev. C* **88**, 064607 (2013).
- [44] A. Ergun et al., a talk at NUFRA2013: International conference on nuclear fragmentation, 29 Sep - 6 Oct 2013, Kemer, Turkey, <http://fias.uni-frankfurt.de/historical/nufra2013>.